Digital-Assisted Asynchronous Compressive Sensing Front-End

Jun Zhou, *Student Member, IEEE*, Mario Ramirez, Samuel Palermo, *Member, IEEE*, and Sebastian Hoyos, *Member, IEEE*

***Abstract*—Compressive sensing (CS) is a promising technique that enables sub-Nyquist sampling, while still guaranteeing the reliable signal recovery. However, existing mixed-signal CS front-end implementation schemes often suffer from high power consumption and nonlinearity. This paper presents a digital-assisted asynchronous compressive sensing (DACS) front-end which offers lower power and higher reconstruction performance relative to the conventional CS-based approaches. The front-end architecture leverages a continuous-time ternary encoding scheme which modulates amplitude variation to ternary timing information. Power is optimized by employing digital-assisted modules in the front-end circuit and a part-time operation strategy for high-power modules. An S-member Group-based Total Variation (S-GTV) algorithm is proposed for the sparse reconstruction of piecewise-constant signals. By including both the inter-group and intra-group total variation, the S-GTV scheme outperforms the conventional TV-based methods in terms of faster convergence rate and better sparse reconstruction performance. Analyses and simulations with a typical ECG recording system confirm that the proposed DACS front-end outperforms a conventional CS-based front-end using a random demodulator in terms of lower power consumption, higher recovery performance, and more system flexibility.**

***Index Terms*—Asynchronous architecture, compressive sensing (CS), continuous-time ternary encoding, digital-assisted front-end, part-time randomization, total variation.**

I. Introduction

EXPLODING bandwidth demand in current wireless applications and standards, such as WirelessHD,[1] IEEE 802.15.3c (WPAN),[2] and IEEE 802.11.ad (WLAN),[3] imposes numerous challenges on system implementations [1]. Systems which utilize traditional analog-to-digital converters (ADC) must have a sampling rate that is at least twice the signal's bandwidth according to the famous Shannon–Nyquist sampling theorem. However, even for designs in advanced technology nodes, high sampling rates usually lead to excessive power consumption and become one of major challenges for portable battery-powered systems [2]–[4]. Although advanced digital signal processing (DSP) methods reduce overall power consumption by decreasing the data rate in energy-demanding radio links [5]–[7], most of these techniques require Nyquist sampling for input. A natural question arises, if the target signal has some special characteristics, such as sparse, compressible, piecewise-constant, etc., is it possible to realize sub-Nyquist sampling without compromising the recovery performance?

Compressive sensing (CS) is a promising technique which enables sub-Nyquist sampling of sparse or compressible signals. According to the CS theorem, any sufficiently sparse and/or compressible signal can be perfectly reconstructed with an overwhelming probability from a much smaller number of incoherent, randomized linear projection samples relative to the Nyquist sampling systems [8], [9]. The CS technique integrates sampling and compression into one step, reducing the sampling directly from the analog front-end. Because of its sub-Nyquist sampling ability, the CS framework has shown potential in many applications, such as medical imaging [10], communications [11], machine learning [12], statistical signal processing [13], and geophysics [14].

Several implementation schemes have been presented for mixed-signal CS front-ends [15]–[21]. As shown in Fig. 1(a), the conventional CS system employs a random demodulator which consists of a pseudorandom number (PN) generator, a mixer, and an integrator [15]–[18]. The mixer performs randomization by multiplying the input with a PN sequence. The integrator operates as an anti-aliasing filter and also serves as a sampling module working at a low rate. Generally, the chipping frequency at the mixer needs to be larger than the Nyquist rate to guarantee incoherent measurements, resulting in considerable dynamic power. In addition, the dedicated analog circuitries are required to display high linearity in measurement generation, as non-linear distortion is difficult to remove in the sparse recovery stage [22]. As both the mixer and integrator are operating in the entire measurement generation, the random demodulator displays excessive dynamic power consumption [15]. An adaptive sampling technique using an integrate-and-fire scheme is proposed in [19]. However, this approach still requires continuous-time waveform chipping and fires even when no signal variation is present. In [20], the authors suggest a digital-assisted CS implementation to replace the high-power modules, such as the mixer and integrator, with their digital counterparts. However, this system is limited to low frequency applications and still requires the PN generator and randomization procedure to operate in a continuous-time mode. An alternative modulated wave converter approach

Manuscript received March 01, 2012; revised August 21, 2012; accepted September 14, 2012. Date of publication November 15, 2012; current version December 05, 2012. This paper was recommended by Guest Editor D. Allstot.

The authors are with Analog & Mixed Signal Center, Department of Electrical & Computer Engineering, Texas A&M University, College Station, TX 77843-3128 USA. (e-mail: ecolejun@tamu.edu; mario.ramirez@neo.tamu.edu; spalermo@ece.tamu.edu; hoyos@ece.tamu.edu).

Color versions of one or more of the figures in this paper are available online at http://ieeexplore.ieee.org.

Digital Object Identifier 10.1109/JETCAS.2012.2222218

[1]WirelessHD. [Online]. Available: http://www.wirelesshd.org

[2]*IEEE 802.15 WPAN Task Group 3c (TG3c): Millimeter Wave Alternative PHY*. [Online]. Available: http://www.ieee802.org/15/pub/TG3c.html

[3]*IEEE 802.11*. [Online]. Available: http://www.ieee802.org/11/Reports/tgad_update.htm

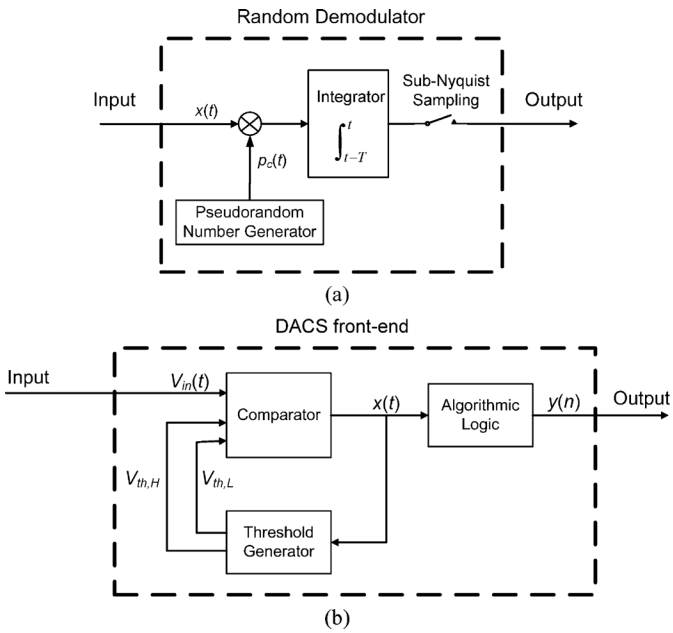

Fig. 1. Block diagram of a mixed-signal CS front-end. (a) Conventional random demodulator. (b) Proposed DACS front-end.

[21] can also achieve sub-Nyquist sampling. But it requires a large number of active channels which is no smaller than four times of the bands, resulting in increased hardware overhead. In addition, it is challenging to implement the hardware for T-periodic waveform generation.

This paper presents a digital-assisted asynchronous compressive sensing (DACS) front-end (Fig. 1(b)) that features reduced power consumption and improved reconstruction performance relative to a conventional mixed-signal CS front-end. A continuous-time ternary-encoding (CT-TE) scheme is proposed to modulate signal amplitude variation into ternary piecewise-constant timing information. By employing digital-assisted modules, part-time randomization is realized in the DACS front-end that results in reduced power consumption. An S-member group-based total variation (S-GTV) algorithm is presented for the sparse recovery of piecewise-constant signals. By including both the inter-group and intra-group TV penalties, the S-GTV scheme outperforms the conventional TV-based method [23] in terms of faster convergence rate and better reconstruction performance.

As a case study, the proposed DACS front-end is evaluated in an ECG recording context in terms of heart rate detection and mean square error of sparse recovery. ECG signals from the MIT-BIH arrhythmia database [24] are used in simulations. Analyses and simulations demonstrate that the proposed DACS front-end outperforms a conventional CS front-end implementation scheme in terms of lower power consumption, higher recovery performance, and more system flexibility.

This paper is organized as follows. Section II briefly reviews the compressive sensing framework. The proposed DACS front-end, including block diagrams of the CT-TE scheme and algorithmic logic, are introduced in Section III. Some non-ideal effects in circuit design are also discussed. Section IV presents the S-GTV algorithm tailored for the sparse reconstruction of piecewise-constant signals. Simulation results and analysis of the DACS front-end in ECG recording application are given in Section V. Finally, Section VI concludes the paper.

II. CS Background

A signal $x \in \mathbb{R}^N$ is called K-sparse or compressible in a representation basis $\{\psi_i\}_{i=1}^N$ if only $K \ll N$ of its coefficients $\{\alpha_i\}_{i=1}^N$ are significant and the rest are zero or negligible by power law. Here we define sparsity as the ratio K/N. In general, compressible signals can be well approximated by sparse signals [25]. Let $\mathbf{\Phi}$ denote an $M \times N$ measurement matrix, where each column of $\mathbf{\Phi}$ is called one atom. Measurements are generated by the linear combination of $\mathbf{\Phi}$ and signal x. Then, the signal recovery problem is

$$\min \|x\|_0 \quad \text{subject to} \quad y = \mathbf{\Phi} x. \tag{1}$$

Problem (1) is known to be combinatorial with NP-hard complexity [8].

Candès *et al.* analyzed that if the measurement matrix $\mathbf{\Phi}$ satisfies the restricted isometry property (RIP) [26],

$$(1 - \delta_K)\|x\|_2^2 \le \|\mathbf{\Phi} x\|_2^2 \le (1 + \delta_K)\|x\|_2^2 \tag{2}$$

for all K-sparse signals $x \in \mathbb{R}^N$ with $\delta_K > 0$ as a constant, the measurement operation $\mathbf{\Phi}$ preserves the Euclidean length of K-sparse signals. Then l_0-norm in problem (1) can be relaxed to l_1-norm.

It is shown in [25] that the measurement matrix $\mathbf{\Phi}$ taken from multiple random processes, such as Gaussian and symmetric Bernoulli (± 1), satisfies RIP with overwhelming probability. In this paper, a measurement matrix drawn from an i.i.d. symmetric Bernoulli distribution is selected due to its easy implementation with a linear feedback shift register (LFSR) circuit [27].

The CS theorem states that a collection of $\mathrm{O}(K \log(N/K))$ incoherent measurements is sufficient for reliable recovery of the original sparse signal [25]. Note that the information rate of any K-sparse signal is on the order of $K \log(N/K)$. Therefore, the CS technique actually samples a sparse signal at its information rate rather than the Nyquist rate.

In literature, many sparse recovery algorithms have been reported for CS systems [28]–[33]. These algorithms and their modifications can be roughly categorized into two groups. One group follows the basis pursuit principle and relaxes the original problem (1) to an l_1-norm optimization problem [28]–[30]

$$\min \|x\|_1 \quad \text{subject to} \quad y = \mathbf{\Phi} x. \tag{3}$$

Note that problem (3) is a convex problem and can be solved in polynomial time. The other group adopts the greedy principle to find the sparse solution by iteration [31]–[33].

III. Digital-Assisted Asynchronous CS (DACS)

The proposed DACS front-end consists of two modules: CT-TE and algorithmic logic. The CT-TE module performs adaptive thresholding and provides algorithmic logic with the

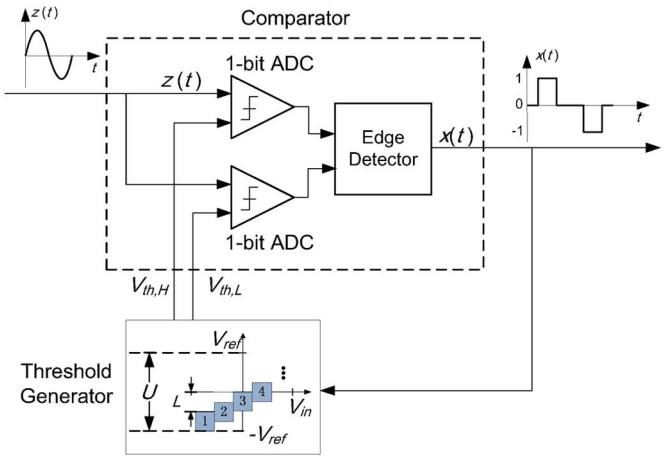

Fig. 2. Block diagram of the CT-TE scheme.

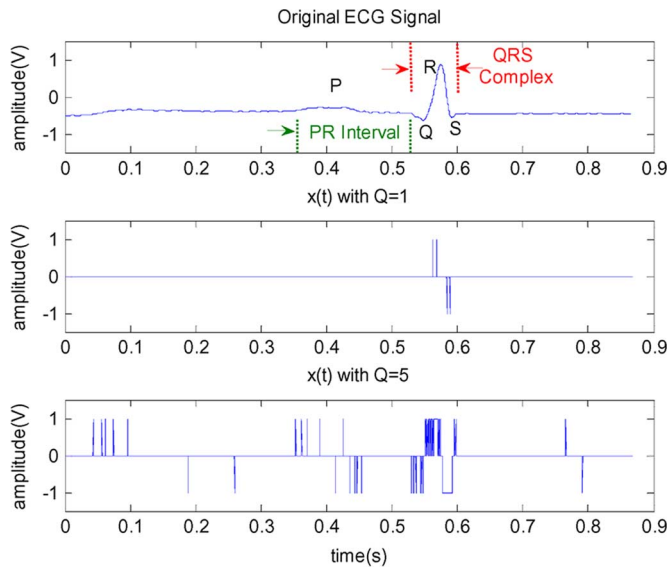

Fig. 3. An example of the CT-TE scheme input and output. From top to bottom, the first waveform shows the original ECG signal. The second waveform shows the output of the CT-TE scheme with $Q = 1$. The third waveform shows the output of the CT-TE scheme when $Q = 5$.

ternary timing information. The algorithmic logic encodes the ternary timing information and generates the randomized measurements at a sub-Nyquist sampling rate.

A. Continuous-Time Ternary-Encoding (CT-TE)

Fig. 2 shows the proposed CT-TE scheme which consists of two parts: a comparator and a threshold generator. Suppose input signal $z(t)$ has been pre-amplified to full-scale with a peak-to-peak value U. $V_{\rm ref}$ denotes the reference signal. The threshold generator divides U equally into 2^Q levels based on quantization bit Q. At each time, it provides a pair of thresholds $(V_{{\rm th},L}, V_{{\rm th},H})$ to the comparator. The difference between $V_{{\rm th},L}$ and $V_{{\rm th},H}$ is a quantization step L. In the ADC context, it's equal to 1 least significant bit (LSB).

The threshold pair $(V_{{\rm th},L}, V_{{\rm th},H})$ forms a comparison window. Initially, the comparison window is set to a quantization level that captures input signal by calculating its running average. When $z(t)$ goes higher than $V_{{\rm th},H}$ or lower than $V_{{\rm th},L}$, the comparator outputs "$+1$" or "-1", respectively and requires the threshold generator to update the comparison window for the next comparison based on the input variation; otherwise, the comparator outputs "0", and the current threshold pair remains unchanged. By this way, the amplitude variation in $z(t)$ is modulated to ternary timing information $x(t)$. Without loss of generality, we assign unit amplitude to "$+1$" and "-1" pulses.

The embedded Schmitt trigger in the threshold generator makes the proposed CT-TE scheme robust to noise. Although this structure requires one additional bit in threshold resolution, we argue that the effective resolution of the comparator is Q-bits. Fig. 3 shows the output of the CT-TE scheme with a typical ECG signal as the input. When $Q = 1$, the pulse in $x(t)$ concentrates around the QRS complex where significant variation occurs. However, $x(t)$ remains 0 for most of other time. Hence, $x(t)$ is a ternary approximation of the original signal with timing information that captures the most significant variation. Here a significant variation means the one that exceeds the given resolution. By increasing Q, the CT-TE scheme increases the ability to detect small variations.

The CT-TE scheme is different from some other modulation methods, like the time encoding machine (TEM) [34], delta modulation [35] and integrate-and-fire scheme [19], which also converts amplitude information into timing information. Both TEM and delta modulation include a negative feedback loop to lock the input signal. Once starting, the entire circuit keeps on flip-flopping, like a sigma-delta modulator output with constant input, and firing all the time even when there is no signal at the input. The integrate-and-fire scheme calculates the running average and also fires even when no variation occurs, resulting in unnecessary power overhead. Whereas in the CT-TE scheme, the circuits fire only when significant variation occurs. As a result, the proposed CT-TE scheme modulates the amplitude variations into timing information more efficiently.

The CT-TE scheme also introduces quantization noise like the conventional ADCs. Obviously, a large quantization bit Q provides high resolution. However, the comparator requires sufficient settling time to provide a stable output and the threshold generator also requires time to update the comparison window properly. Therefore, the achievable Q is constrained by the slew rate of signal and the settling time of the circuitry. Let *SR* denote the slew rate of the input signal $z(t)$.

$$SR = \max\left(\left|\frac{dz(t)}{dt}\right|\right) \tag{4}$$

Assuming that the settling time of the entire circuitry is σ, we have a maximum allowable Q of

$$Q \le \log_2 \frac{U}{SR \cdot \sigma} - 1. \tag{5}$$

If the CT-TE module in Fig. 2 violates (5), $x(t)$ cannot provide sufficient pulses to represent a variation larger than $2L$ due to the ternary output in each comparison. As a result, $x(t)$ is not able to track fast variations. This phenomenon is referred to as overflow distortion. Hence, the condition of (5) should be satisfied in order to guarantee the recovery of $z(t)$ from $x(t)$.

In addition to the finite response rate, for small input signals the comparator can enter into a metastable state and fails

to resolve within the assigned time. This unpredictability of the comparator can cause errors in the subsequent logic. In order to quantify the probability of a metastability error, we analyze the step response of a typical two-stage open-loop comparator with a DC gain of $A_{\rm DC}$ [36]. Its frequency response is

$$A_v(s) = \frac{A_{\rm DC}}{\left(\frac{s}{p_1}+1\right)\left(\frac{s}{p_2}+1\right)}, \tag{6}$$

where p_1 and p_2 are the comparator's two poles. The step response when $p_1 \neq p_2$ is

$$v_{\rm out}(t) = A_{\rm DC} v_{\rm in}\left[1 + \frac{p_2}{p_1-p_2}e^{-p_1 t} - \frac{p_1}{p_1-p_2}e^{-p_2 t}\right]. \tag{7}$$

Assuming a uniform input signal distribution, the probability of metastability error $P_{\rm err}$ by the end of settling time σ is

$$P_{\rm err} = \frac{2(2^Q-1)V_L}{A_{\rm DC}U\left[1+\frac{p_2}{p_1-p_2}e^{-p_1\sigma} - \frac{p_1}{p_1-p_2}e^{-p_2\sigma}\right]} \tag{8}$$

where V_L is the valid logic level. Note that a small Q decreases the probability of metastability error.

In order to suppress the metastability in the Edge Detector unit in Fig. 2, we can employ a double pass-transistor logic (DPL) [37] which has potential for high-speed design due to its low input capacitance. Also, the DPL provides dual logic paths for every logic function. It introduces additional robustness to track amplitude variation.

Comparator offset is another important issue. A static offset displays a compression or extension to each of the piecewise-constant section of $x(t)$, with an extreme case being when the offsets in the two 1-bit ADCs reach to one quantization step L. In such a case, the comparator in Fig. 2 may be unstable. While auto-zeroing techniques [38] can effectively reduce this input offset, ultimately this is limited by circuit non-idealities such as charge injection. Hence, the maximum Q is jointly determined by (5), (8), and offset considerations.

B. Algorithmic Logic

With proper Q and σ, the output of the CT-TE scheme, $x(t)$, exhibits ternary piecewise-constant characteristics, i.e., $x(t) = \{-1, 0, 1\}$. A discrete set of time $\boldsymbol{T} = \{T_0, T_1, T_2 \ldots\}$, represents the time instants of each transition edge in $x(t)$. Since $x(t)$ has only three possible values, two thresholds are sufficient for the transition edge detection. Note that no clock is involved in either the CT-TE module or transition time $\boldsymbol{T}$ detection. Their outputs are fully signal-driven and functions of continuous time. These two circuits are operating in asynchronous mode.

In this architecture, we are more interested in the time period between successive transition edges rather than $\boldsymbol{T}$. Let $T_{i\to i+1}$ denote the time period between ith and $(i+1)$th transition. $T_{i\to i+1}$ can be calculated by counting the elapsed clock cycles $C_{i\to i+1}$ that runs at a predefined frequency f_c,

$$T_{i\to i+1} = C_{i\to i+1}\Delta t \tag{9}$$

where $\Delta t = 1/f_c$. Usually f_c is higher than the Nyquist rate of the input signal to provide sufficient timing resolution.

As described in Section II, compressive sensing modulates a signal into incoherent measurements by a linear projection and then recovers it from a reduced number of measurements relative to a Nyquist sampling system. The measurement generation in (3) includes two operations: randomization and integration. For a piecewise-constant signal, we have following transformation in each constant section.

$$\int_{T_i}^{T_{i+1}} x(t)\cdot p_c(t)dt = x(t)\cdot\int_{T_i}^{T_{i+1}} p_c(t)dt \tag{10}$$

where $p_c(t)$ stands for the chipping sequence from the PN generator. In a random demodulator, the mixer and integrator are required to operate continuously during the measurement generation. By (10), with the accumulated chipping waveform, a single multiplication is sufficient for each constant section. Because $p_c(t)$ is a discrete sequence in the CS front-end, multiplication and integration in (10) can be efficiently implemented by a multiplier and an accumulator in digital circuitry rather than employing a dedicated mixer and integrator in the analog domain. As shown in [15], the random sequence demands significant buffering effort before being applied to the mixer, resulting in more static power consumption. By leveraging the piecewise-constant property, the algorithmic logic enjoys the advantages of digital circuitry scaling, such as smaller area, lower static power consumption, and more robustness to nonlinearity, etc.

Moreover, power can be further optimized by shutting down the Pseudorandom Number (PN) generator during the time period when $x(t) = 0$, because the inner product of 0 with any waveform is trivial. Therefore, the PN generator is active only when $x(t) = \pm 1$ in our algorithmic logic; otherwise it is deactivated. Since the PN generator must operate at a higher frequency than the Nyquist rate of input signal [25], a part-time randomization scheme optimizes the operating time of the LFSR. As reported in [15], the combination of PN sequence generation and randomization procedure accounts for nearly half of the entire power consumption in a random demodulator. The part-time operation strategy for high-power modules can directly reduce the on-chip power during the measurement generation.

Though the aforementioned part-time randomization scheme is attractive, it may prohibit the sparse signal recovery in (3). The reason is that we discard all zero-valued sections in $x(t)$. Randomization is actually performed on a concatenated signal with nonzero-valued sections in $x(t)$ rather than the original one. As a consequence, the timing information of all zero-valued sections is missing during sampling. Therefore, detailed timing information of such part-time randomization must be provided in measurements to ensure the exact reconstruction.

Recall that $x(t)$ is a ternary piecewise-constant signal with unit amplitude in nonzero-valued sections. The length of a certain zero-valued section in $x(t)$ can be modulated to the amplitude of its next nonzero-valued section without blurring any amplitude information. Fig. 4 shows the block diagram of the proposed algorithmic logic in the DACS front-end. The edge detector locates the transition edges in the input $x(t)$. The output timing information $\boldsymbol{T}$ is provided to the PN generator for part-time randomization, and also to the counter for calculation of

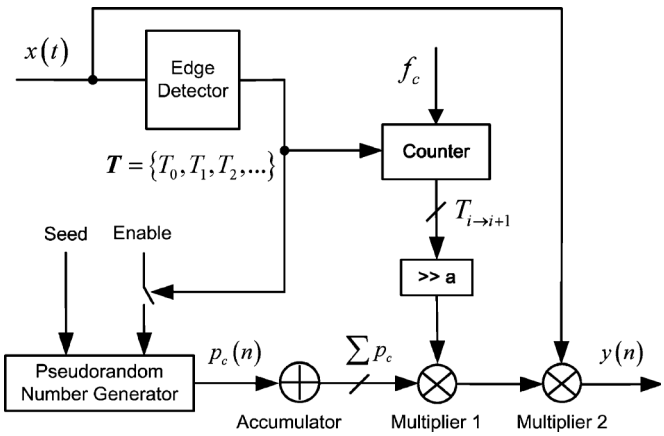

Fig. 4. Block diagram of the algorithmic logic in the DACS front-end.

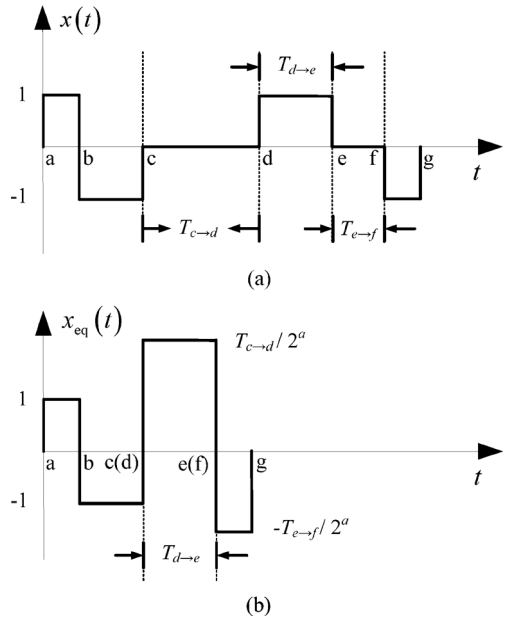

Fig. 5. An example of the equivalent signal for randomization in the DACS front-end. (a) Original ternary piecewise-constant signal. (b) Equivalent compact signal.

zero-valued section length. Suppose T_i and T_{i+1} stand for the beginning and ending transition time of a zero-valued section. The length of this zero-valued section, $T_{i\to i+1}$, is modulated to the amplitude of its next nonzero-valued section by Multiplier 1 in Fig. 4. A coefficient a is added to adjust the level of timing information. Meanwhile, the PN generator stops and holds the state at T_i. After finishing the amplitude modulation, the counter should be reset to prepare for the next zero-valued section. At this time, the PN generator resumes working and starts from its current state. Multiplier 2 adjusts the sign of measurement and finalizes the measurement generation.

Since randomization is performed on a concatenated signal rather than the original one $x(t)$, it is worthy to look at the equivalent signal $x_{\rm eq}(t)$ for the randomized measurements. We refer to $x_{\rm eq}(t)$ as the equivalent compact form of $x(t)$, shown in Fig. 5. Suppose the output of the CT-TE scheme $x(t)$ has a waveform shown in Fig. 5(a). Then the edge detector finds each transition edge in $x(t)$. In this paper, we assume the edge detector has been properly design to detect all transition edges in $x(t)$. For convenience, we mark them from a to g. During the nonzero-valued sections, the counter keeps silent and the equivalent compact signal $x_{\rm eq}(t)$ just copies the input to output, like sections (a, b) and (b, c). When zero-valued section (c, d) comes, the counter starts calculating its length $T_{c\to d}$, which is later on modulated to the amplitude of its next section (d, e), as shown in Fig. 5(b). Similar operations are carried out on section (f, g). The final equivalent compact signal $x_{\rm eq}(t)$ is shown in Fig. 5(b). Note that, $x_{\rm eq}(t)$ is no longer a ternary signal like $x(t)$. However, $x_{\rm eq}(t)$ is piecewise-constant and able to include all the information of the original $x(t)$ during the measurement generation.

In order to quantify the percentage of part-time operation, we define the part-time ratio as the total randomization time of the equivalent compact signal $x_{\rm eq}(t)$ over that of the original ternary signal $x(t)$

$$r_{\rm part-time} = \frac{\sum_{i\in x_{\rm eq}} T_{i\to i+1}}{\sum_{i\in x} T_{i\to i+1}}. \tag{11}$$

It is worthy to point out the DACS front-end has very high efficiency for time-sparse signals, e.g., ECG signal, ultra-wide band (UWB) pulse signal, radar system, ultrasound signal, etc. This is because the DACS front-end targets at amplitude variation and enables part-time operation of power-demanding modules which otherwise should be always on, such as the random demodulator. Besides, the proposed DACS front-end is not restricted to time-sparse signals. For example, tone signals also have equivalent compact signals $x_{\rm eq}(n)$ with the DACS front-end. Then, all signal processing presented previously can be directly applied. However, the efficiency decreases when a signal is sparse in other domain rather than time domain, because the part-time ratio decreases as the signal activity increases.

IV. S-Member Group-Based Total Variation

In this section, we present an S-member Group-Based TV (S-GTV) scheme for sparse recovery of the piecewise-constant timing information $x(t)$ from the noise corrupted measurements. Before introducing the proposed S-GTV scheme, we first define the concept of "group" adopted in this paper.

Definition 1: In the discrete setting, group is a collection of consecutive points that have the similar amplitude information.

S-member means the maximal group size is S. Including both the inter-group and intra-group total variation of $x \in \mathbb{R}^N$, our goal is to minimize the objective function in

$$J(x) = \alpha {\rm TV}(x) + \gamma {\rm GTV}(x, S) + \|y - Ax\|_2^2 \tag{12}$$

with the following constraints:

$$\begin{aligned} &{\rm TV}(x) = \|Dx\|_1 \\ &{\rm GTV}(x, S) = \sum_{i=1}^{N} \|Dx_i^{i+S_i-1}\|_1 \\ &S_i = \min(S, g_i) \\ &g_i = \arg\max_g \left(\|Dx_i^{i+g}\|_\infty \le TH < \|Dx_i^{i+g+1}\|_\infty \right) \end{aligned} \tag{13}$$

where D is the gradient matrix, A is a bounded linear operator, α and γ are tuning parameters that balance TV and GTV penalties, x_i^j means the string comprising samples i through j within x, g_i is the group size seeing from ith sample, and *TH* is the threshold for similarity.

We adopt the Iteratively Reweighted Least Squares (IRLS) method [39] in sparse recovery. As shown in [39], the l_p-norm $(p \geq 1)$ can be approximated by the weighted l_2-norm at each iteration step. Then, the optimization problem in (12) can be approximated by a least squares problem in each iteration.

Comparing with the conventional TV-based method, S-GTV includes a new regularization term GTV(x, S) that measures the intra-group total variation. Since it's the summation of a set of l_1-norm, each one is approximated individually. The difference lies in the weights calculation. In the proposed S-GTV scheme, each sample in x has S weights corresponding to its S neighbors. Depending on the group size limit and signal characteristics, the actual number of neighbors involved in the group-based TV calculation varies among different samples. The processing of S-GTV scheme is illustrated in Algorithm 1.

For initialization, the weights $W^j(i)$ for the jth neighbor is set to 1, where $i = 1, 2, \ldots, N$ and $j = 1, 2, \ldots, S$. In each iteration, an equivalent total variation W_{total} is calculated by least squares approximation. Note that W_{total} includes both the inter-group and intra-group total variation described in (13). By tuning the parameters α and γ, we can control the direction of optimization. Specifically, a smaller γ gives more freedom to the optimizer to seek the significant point-wise variations or local variations; while a larger γ leads the optimizer to the piecewise-constant sections or global variations.

It is worthy to point out the sparse recovery of problem (12) is $x_{\text{eq}}(n)$ rather than $x(n)$. After amplitude compensation, the equivalent compact signal $[a * x_{\text{eq}}(n)]$ should have integer-valued amplitude because both $\sum p_c$ and $T_{i \to i+1}$ are integers by default. Then, $[a * x_{\text{eq}}(n)]$ is rounded to integers to reconstruct the original ternary piecewise-constant signal $x(n)$. If the absolute amplitude of a certain piecewise-constant section is larger than 1, i.e., $|a * x_{\text{eq}}(i)| > 1$, it implies there is a zero-valued section before it. Also, the length of this zero-valued section is equal to $|a * x_{\text{eq}}(i)|$ with the same sign of $[a * x_{\text{eq}}(n)]$. For sections with unit amplitude, they are copied to the output directly.

Algorithm 1: S-member Group-Based Total Variation

INPUT: the randomization matrix $\mathbf{\Phi}$, the received signal y, the threshold *TH*, the maximal group size S, the maximal iteration number *imax*, and the tuning parameters α and γ.

OUTPUT: the estimation of piecewise-constant signal $\hat{x}$

PROCEDURE:

1. Initialize the estimate signal $x_{t-1} = 0$, the weight $W_{t-1}^j = 1$ for jth neighbor, and the iteration count $t = 1$
2. **while** $t \leq imax$, **do**
3. Find the gradient of $x, x' = Dx$.
4. Perform thresholding find group size for each sample, $g_i = \min\{S, \arg\max_g |x'^{i+g}_i|_\infty \leq TH < |x'^{i+g+1}_i|_\infty\}$.
5. Calculate the weight for the least squares approximation $W_{\text{total}}(i) = \alpha D' W_{t-1}^1(i) D + \gamma \sum_{j=1}^{g_i} D_j^{'} W_{t-1}^j(i) D_j$, where D_j is j-shifted gradient matrix.
6. Calculate the Least Squares solution for current iteration, $x_t = (\mathbf{\Phi}' * \mathbf{\Phi} + W_{\text{total}})^{-1} * \mathbf{\Phi}' y$
7. Update the weight of all neighbors, $W_t^j = 2 * \text{diag}(1/D_j x_t)$
8. Increment t
9. **end while**
10. **return** $\hat{x} \leftarrow x_t$

Accurate recovery of zero-valued sections is important, as a small error results in a shift of the peak (e.g., the QRS complex), and may cause a large overall reconstruction error. This work proposes two compensation techniques to ensure sufficient recovery performance. The first technique utilizes an intra- group TV penalty in the proposed S-GTV scheme. Recall that the iteration process in Algorithm 1 starts from randomized measurements. It is reasonable to use a smaller γ in the beginning to figure out a "contour" of the piecewise-constant approximation. After that, increasing γ will smooth out noise and simultaneously expedite the convergence rate. The second technique leverages the property that the PN generator clock rate is larger than the input Nyquist rate. If we have an H times higher clock rate, a single activity in the CT-TE scheme ("+1" or "−1") results in at least H discrete samples and each piecewise-constant section in $x(n)$ should have a minimum of H samples. As will be shown in Section V, it is possible to correct some outliers in the reconstruction result with compensation.

V. Analysis

In order to analyze the performance of the DACS front-end, a 1-channel version (Fig. 1(b)) is constructed. A typical ECG signal from the MIT-BIH arrhythmia database [24] is used as a case study for illustration. In the following simulations, one complete cycle is simulated.

Recall from Section III that the CT-TE module operates in an asynchronous mode. While there is no explicit sample and hold clock in the DACS front-end, the comparators' finite settling time limits both the maximum response rate to input variation and the maximum resolution. From (5), Q is upper-bounded by the signal's slew rate and circuit settling time, σ. Assuming a comparison rate of $1/\sigma$ and a full-scale ECG signal of 2 V_{pp} and 100 V/s slew rate, the relationship between the minimum comparison rate and the quantization bit Q is shown in Fig. 6. As Q increases, the required comparison rate of the CT-TE module increases exponentially. Hence, high-speed CT-TE circuitry is required for a high-resolution DACS front-end. For example, if the comparison rate is 100 kHz, the maximum quantization bit Q can be 10. In order to focus on the performance of the proposed DACS front-end and S-GTV recovery algorithm, the following analysis assumes that the CT-TE circuitry supports 10-bit resolution:

As shown previously in Fig. 3, the number of significant variations increases as the quantization bit Q goes up due to the observation window becoming narrow when Q is large. The

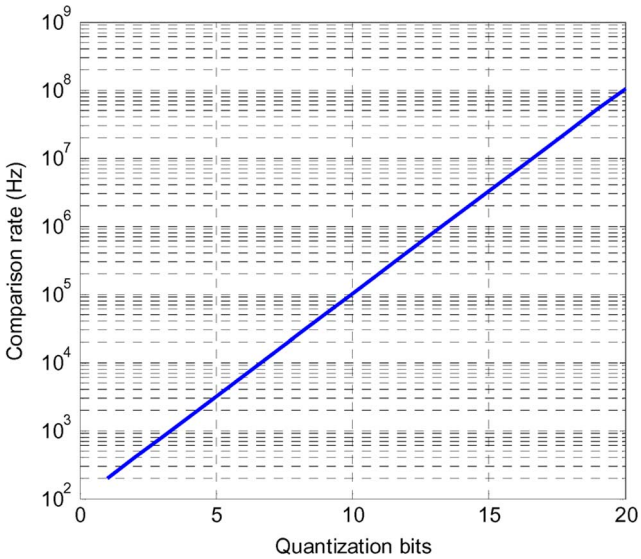

Fig. 6. Relationship between minimal comparison rate and quantization bits for typical ECG signals.

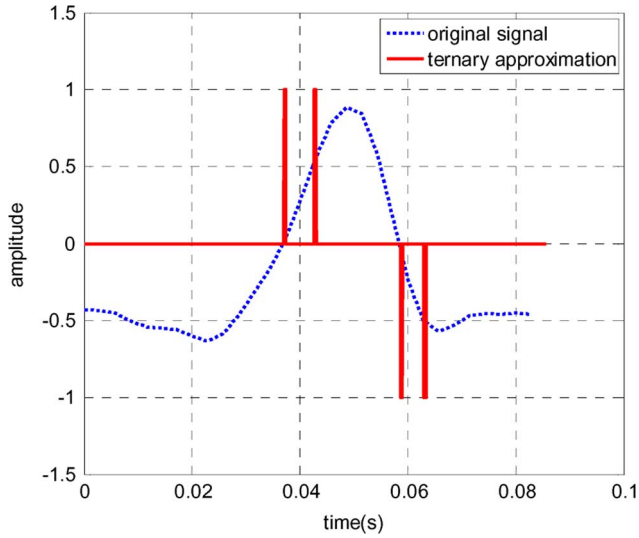

Fig. 8. Original waveform of QRS complex and its ternary approximation by CT-TE scheme, $Q = 1$.

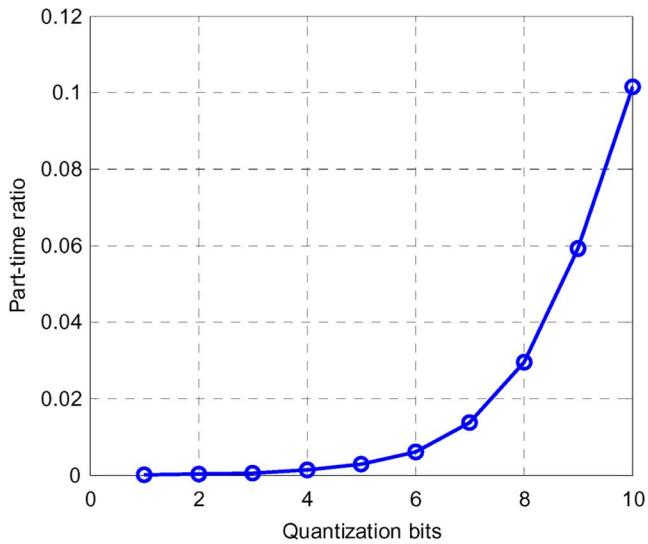

Fig. 7. Relationship between part-time ratio and quantization bits for ECG signal.

part-time randomization strategy discussed in Section III is applicable to the zero-valued sections and thus it is informative to investigate the relationship between the part-time ratio and quantization bit. Fig. 7 shows that the part-time ratio increases as Q increases due to the detection of small input variations. As the resolution approaches the noise floor, this also increases the part-time ratio. However, even with $Q = 10$ the part-time ratio is still around 0.1 for the ECG signal; suggesting a very efficient DACS front-end implementation.

The highly digital DACS front-end provides multiple attractive properties for current and future applications. By replacing the dedicated analog modules in random demodulator implementations, such as the mixer and integrator, with their digital counterparts, the DACS front-end will scale well with CMOS processes and provide increased robustness to nonlinearity. A primary advantage of the proposed DACS front-end compared to other digital-assisted designs [20] results from the part-time randomization which optimizes the operation of the PN generator, which is typically the highest power digital block. In [20], the accumulator keeps on operating during measurement generation. While in the DACS front-end, accumulator is shut down for zero-valued sections. Instead, a counter working at the same rate is employed. If accumulator and counter have the similar toggling rate, they have comparable power consumption. Then, the shorter operating time of PN generator reduces the overall on-chip power consumption. The small part-time ratio shown in Fig. 7 shows the power savings potential of the DACS front-end.

In order to evaluate the sparse recovery of conventional TV-based methods and the S-GTV algorithm, we utilize the QRS complex which represents the most significant variation region in an ECG signal. Fig. 8 shows the original QRS complex and its ternary timing information $x(n)$ after the CT-TE scheme when $Q = 1$. Here we define the sub-Nyquist sampling ratio (SSR) in (14), where f_{Nyq} is the Nyquist rate and f_s is the actually sampling rate.

$$\mathrm{SSR} = \frac{f_s}{f_{\mathrm{Nyq}}}. \tag{14}$$

Setting the SSR to 0.18, Figs. 9–11 show the sparse recovery of the equivalent compact signal $x_{\mathrm{eq}}(n)$ using the conventional TV method and the S-GTV scheme at different signal-to-noise ratios (SNRs). In the noise-free case, Fig. 9(a) shows that both the conventional TV method and the S-GTV scheme can exactly recover $x_{\mathrm{eq}}(n)$. However, as shown in Fig. 9(b), by evaluating the mean squares error (MSE) at each iteration step, the proposed S-GTV scheme exhibits a faster convergence relative to the conventional TV approach. This is because as the minimizer approaches to the optimum, the GTV term regularizes the objective function to a direction that favors the piecewise-constant estimation, expediting the convergence rate. In Fig. 9(b), an error floor is observed in both the conventional TV and S-GTV scheme due to the small additive offset introduced

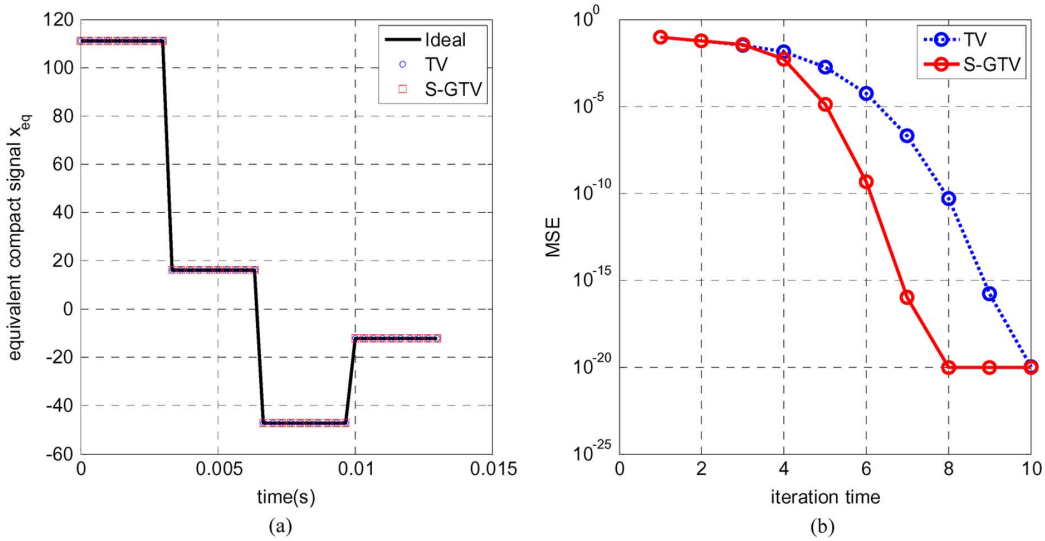

Fig. 9. Sparse recovery of piecewise-constant signal $x_{\mathrm{eq}}(n)$ by conventional TV-based method and S-GTV scheme in noise-free case. (a) Waveform recovery. (b) MSE versus iteration time.

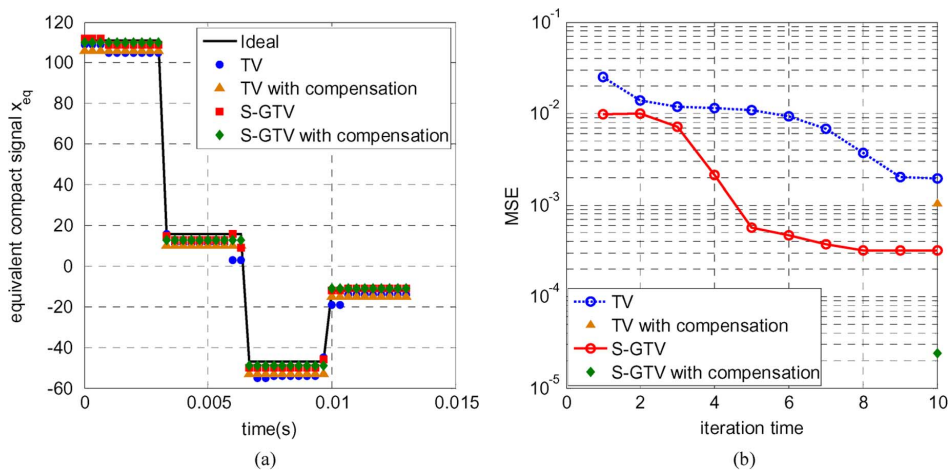

Fig. 10. Sparse recovery of piecewise-constant signal $x_{\mathrm{eq}}(n)$ by conventional TV-based method and S-GTV scheme when $\mathrm{SNR} = 40$ dB. (a) Waveform recovery. (b) MSE versus iteration time.

in Step 6 of Algorithm 1 which ensures the inverse operation is tractable in the numerical calculation.

Fig. 10 shows that the S-GTV algorithm exhibits better MSE performance compared to the conventional TV-based method when SNR decreases to 40 dB. This difference results from the combination of intra-group and inter-group TV penalties in the S-GTV scheme. Although group TV penalty can not eliminate outliers completely in the expected piecewise-constant sections, the compensation techniques proposed in Section IV ensure an accurate recovery of the equivalent compact signal $x_{\mathrm{eq}}(n)$. In Fig. 10, MSE displays an 11.3 dB improvement with the S-GTV scheme with compensation.

Fig. 11 shows that both the conventional TV approach and S-GTV algorithm have very limited MSE performance without compensation when noise increases to 20 dB SNR. Compared to the conventional TV approach, the S-GTV scheme is good at recovering large piecewise-constant sections. While outliers do exist in the sparse recovery result, the S-GTV scheme with compensation is able to guarantee the demodulation process of ternary timing information. By exploiting the characteristics of the equivalent compact signal, we can roughly categorize the entire recovery into three groups: one group with amplitude less than -1, one group with amplitude larger than 1, and one that includes all others. For the first two groups, the amplitude of consecutive samples can be averaged, which represents the length of the zero-valued section before it. While for the third group, the amplitude is around 1 or -1. Fig. 12 illustrates the sparse recovery with the compensation technique when $\mathrm{SNR} = 20$ dB and the ideal noise-free case. These results suggest that the proposed S-GTV scheme achieves an accurate recovery of ternary timing information with the compensation techniques. Once the ternary timing signal is obtained, the original signal can be reconstructed by integration and/or advanced smoothing techniques. For illustration, we adopt a cascaded integrator-comb filter (CIC) for running average computation in the following simulations.

Fig. 13 shows the waveform reconstructions of the QRS complex by the DACS front-end, with 1-bit and 3-bit schemes simu-

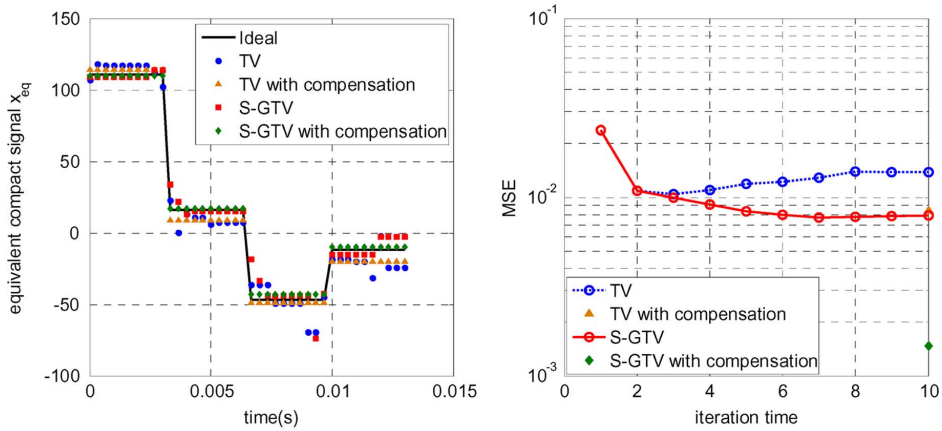

(a) (b)

Fig. 11. Sparse recovery of piecewise-constant signal $x_{\mathrm{eq}}(n)$ by conventional TV-based method and S-GTV scheme when $\mathrm{SNR} = 20$ dB. (a) Waveform recovery. (b) MSE versus iteration time.

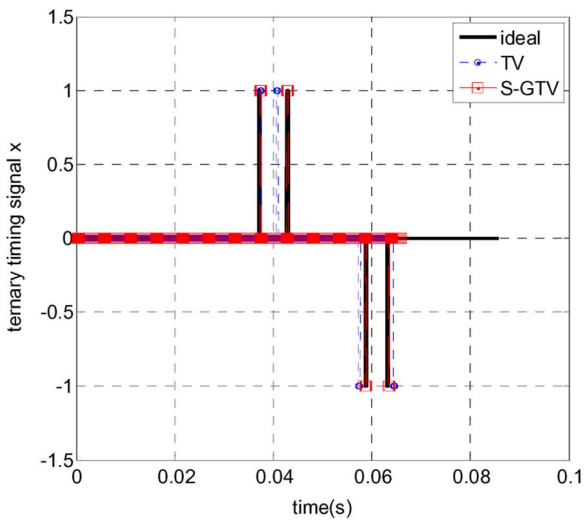

Fig. 12. Recovery of ternary timing signal $x(n)$ with compensation technique.

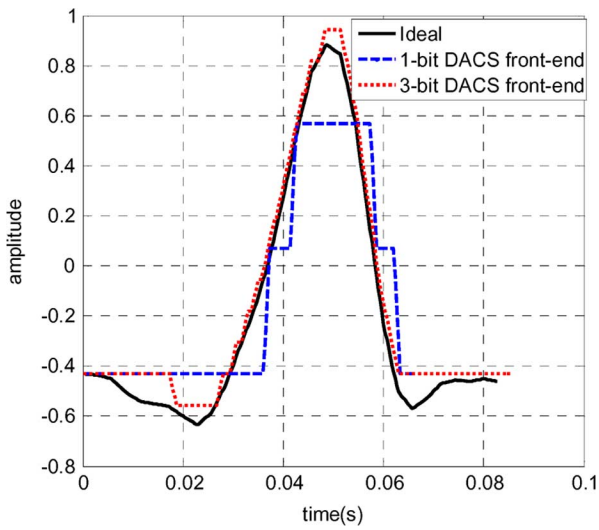

Fig. 13. Waveform reconstruction of QRS complex by DACS front-end with different number of quantization bits.

lated. In the proposed DACS front-end, the amplitude variations are modulated into timing information. Similar to conventional ADCs, the CT-TE scheme also introduces quantization noise which manifests both as small offsets between the ideal waveform and the reconstructed one and as asymmetries between positive and negative sides. Increasing Q improves the resolution and reduces the quantization noise, as shown in Fig. 13.

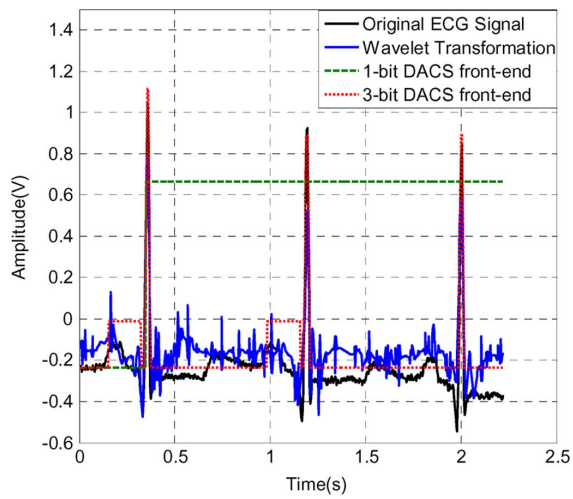

Fig. 14. Waveform reconstruction of ECG pulses by the DACS front-end with different number of quantization bits.

Heart rate detection is a basic function in ECG recording systems and many heart diseases like arrhythmia can be identified from an abnormal heart rate. In Fig. 14, a sequence of 3 heart beat cycles is adopted to evaluate the heart rate detection with 1-bit and 3-bit DACS front-ends with SSR set to 0.18 and SNR set to 20 dB. For comparison, we also include the 3-bit sparse representation using Daubechies wavelets (db4) as a benchmark. As shown in Fig. 14, both the wavelet transformation and the DACS front-end enable sub-Nyquist sampling with a CS technique and the sparse reconstructions of both methods provide reliable heart rate detection with a simple thresholding scheme. It is worth pointing out that the proposed DACS front-end can be initialized to 1-bit quantization for heart rate detection at a very low data rate, as suggested by Fig. 7. Once an abnormal heart rate is identified, more quantization bits can be dynamically assigned to increase the resolution for further analysis. Such a need-based strategy increases the autonomy of the DACS front-end in an ECG recording system and optimizes the power consumption from a system perspective.

VI. Conclusion

This paper presented a DACS front-end for the mixed-signal CS system. The proposed DACS front-end modulates amplitude variation into timing information. By leveraging a CT-TE scheme, the DACS front-end employs digital-assisted circuitry in the analog front-end and realizes part-time randomization in measurement generation. Power consumption is optimized by utilizing the minimal-size digital circuits and reducing the operating time of high-power modules. By packaging the timing information into a compact equivalent, the sampling rate for reconstruction is optimized. An S-member Group-Based Total Variation (S-GTV) algorithm is proposed for the sparse recovery of piecewise-constant signals. The DACS front-end outperforms the conventional CS-based front-ends in terms of lower power consumption, higher signal fidelity, and system flexibility.

References

[1] D. Cabric, M. S. W. Chen, D. A. Sobel, J. Yang, and R. W. Brodersen, "Future wireless systems: UWB, 60 GHz, and cognitive radios," in *IEEE Custom Integr. Circuits Conf.*, 2005, pp. 793–796.

[2] R. H. Walden, "Analog-to-digital converters survey and analysis," *J. Sel. Areas Commun.*, Apr. 1999.

[3] K. Lahiri, A. Raghunathan, S. Dey, and D. Panigrahi, "Battery-driven system design: A new frontier in low power design," in *Proc. IEEE ASPDAC*, Jan. 2002, pp. 261–267.

[4] J. D. Boeck, "Game-changing opportunities for wireless personal healthcare and lifestyle," in *IEEE Int. Solid-State Circuits Conf. (ISSCC)*, 2011, pp. 15–21.

[5] L. Brechet, M. F. Lucas, C. Doncarli, and D. Farina, "Compression of biomedical signals with mother wavelet optimization and best-basis wavelet packet selection," *IEEE Trans. Biomed. Eng.*, vol. 54, no. 12, pp. 2186–2192, Dec. 2007.

[6] Z. M. Liu, Z. X. Xiong, Q. Wu, Y. P. Wang, and K. Castleman, "Cascaded differential and wavelet compression of chromosome images," *IEEE Trans. Biomed. Eng.*, vol. 49, no. 4, pp. 372–383, Apr. 2002.

[7] G. Z. Yang, *Body Sensor Networks*. London, U.K.: Springer, 2006.

[8] E. J. Candès and M. B. Wakin, "An introduction to compressive sampling," *IEEE Signal Process. Mag.*, vol. 25, no. 2, Mar. 2008.

[9] D. Donoho, "Compressed sensing," *IEEE Trans. Inf. Theory*, vol. 52, no. 4, pp. 1289–1306, Apr. 2006.

[10] J. P. Haldar, D. Hernando, and Z. P. Liang, "Compressed-sensing MRI with random encoding," *IEEE Trans. Med. Imag.*, vol. 30, no. 4, pp. 893–903, Apr. 2011.

[11] G. Taubock and F. Hlawatsch, "A compressed sensing technique for OFDM channel estimation in mobile environments: Exploiting channel sparsity for reducing pilots," in *Proc. IEEE Int. Conf. on Acoust., Speech, Signal Process.(ICASSP)*, Apr. 2008, pp. 2885–2888.

[12] J. Wright, A. Yang, A. Ganesh, S. Shastry, and Y. Ma, "Robust face recognition via sparse representation," *IEEE Trans. Pattern Anal. Mach. Intell.*, vol. 31, no. 2, pp. 210–227, Feb. 2009.

[13] M. A. Davenport, P. T. Boufounos, M. B. Wakin, and R. Baraniuk, "Signal processing with compressive measurements," *IEEE J. Sel. Topics in Signal Process.*, vol. 4, no. 2, pp. 445–460, Apr. 2010.

[14] S. Hu *et al.*, "Compressed sensing for resolution enhancement of hyperpolarized 13C flyback 3D-MRSI," *J. Magn. Resonance*, vol. 192, no. 2, pp. 258–264, June 2008.

[15] X. Chen, Z. Yu, S. Hoyos, B. M. Sadler, and J. Silva-Martinez, "A sub-Nyquist rate sampling receiver exploiting compressive sensing," *IEEE Trans. Circuits Syst. I, Reg. Papers*, vol. 58, no. 3, pp. 507–520, Mar. 2011.

[16] H. Mamaghanian, N. Khaled, D. Atienza, and P. Vandergheynst, "Compressed sensing for real-time energy-efficient ECG compression on wireless body sensor nodes," *IEEE Trans. Biomed. Eng.*, vol. 58, no. 9, pp. 2456–2466, Sep. 2011.

[17] E. G. Allstot, A. Y. Chen, A. M. R. Dixon, D. Gangopadhyay, and D. J. Allstot, "Compressive sampling of ECG bio-signals: Quantization noise and sparsity considerations," in *IEEE Biomed. Circuits Syst. Conf.*, 2010, pp. 41–44.

[18] L. F. Polania, R. E. Carrillo, M. B. Velasco, and K. E. Barner, "Compressed sensing based method for ECG compression," in *Proc. IEEE Int. Conf. on Acoust., Speech, Signal Process. (ICASSP)*, Apr. 2011, pp. 761–764.

[19] A. S. Alvarado and J. C. Principe, "From compressive to adaptive sampling of neural and ECG recordings," in *Proc. IEEE Int. Conf. on Acoust., Speech, Signal Process. (ICASSP)*, Apr. 2011, pp. 633–636.

[20] F. Chen, A. P. Chandrakasan, and V. Stojanovic, "A signal-agnostic compressed sensing acquisition system for wireless and implantable sensors," in *IEEE Custom Integr. Circuits Conf.*, Sept. 2010, pp. 1–4.

[21] M. Mishali and Y. C. Eldar, "From theory to pratice: Sub-Nyquist sampling of sparse wideband analog signals," *IEEE J. Sel. Topics Signal Process.*, vol. 4, no. 2, pp. 375–391, Apr. 2010.

[22] Z. Yu, J. Zhou, M. Ramirez, S. Hoyos, and B. M. Sadler, "The impact of ADC nonlinearity in a compressive sensing receiver for frequency-domain sparse signals," *J. Phys. Commun.*, vol. 5, no. 2, pp. 196–207, June 2012.

[23] L. Rudin, S. Osher, and E. Fatemi, "Nonlinear total variation based noise removal algorithms," *Phys. D*, vol. 60, pp. 259–268, 1992.

[24] "MIT-BIH arrhythmia database," 2005 [Online]. Available: http://www.physionet.org/physiobank/database/mitdb/

[25] J. A. Tropp, J. N. Laska, M. F. Duarte, J. K. Romberg, and R. G. Baraniuk, "Beyond Nyquist: Efficient sampling of sparse bandlimited signals," *IEEE Trans. Inf. Theory*, vol. 56, no. 1, pp. 520–544, Jan. 2010.

[26] E. Candès and T. Tao, "Decoding by linear programming," *IEEE Trans. Inf. Theory*, vol. 51, no. 12, pp. 4203–4215, Dec. 2005.

[27] R. S. Katti, X. Ruan, and H. Khattri, "Multiple-output low-power linear feedback shift register design," *IEEE Trans. Circuits Syst. I, Reg. Papers*, vol. 53, no. 7, pp. 1487–1495, July 2006.

[28] E. Candès, J. Romberg, and T. Tao, "Robust uncertainty principles: Exact signal reconstruction from highly incomplete frequency information," *IEEE Trans. Inf. Theory*, vol. 52, no. 2, pp. 489–509, Feb. 2006.

[29] Y. C. Eldar, P. Kuppinger, and H. Bolcskei, "Compressed sensing of block-sparse signals: Uncertainty relations and efficient recovery," *IEEE Trans. Signal Process.*, vol. 58, no. 6, pp. 3042–3054, 2010.

[30] W. Lu and N. Vaswani, "Modified basis pursuit denoising for noisy compressive sensing with partially known support," in *Proc. IEEE Int. Conf. on Acoust. Speech, Signal Process. (ICASSP)*, Apr. 2010, pp. 3926–3929.

[31] J. A. Tropp and A. C. Gilbert, "Signal recovery from random measurements via orthogonal matching pursuit," *IEEE Trans. Inf. Theory*, vol. 53, no. 12, pp. 4655–4666, Dec. 2007.

[32] D. Needell and J. A. Tropp, "CoSaMP: Iterative signal recovery from incomplete and inaccurate samples," *Appl. Computat. Harmonic Anal.*, vol. 26, no. 3, pp. 301–321, 2009.

[33] Z. B. Haim and Y. C. Eldar, "Near-oracle performance of greedy block-sparse estimation techniques from noisy measurements," *IEEE J. Sel. Topics in Signal Process.*, vol. 5, no. 5, pp. 1032–1047, Sep. 2011.

[34] A. A. Lazar and L. T. Toth, "Perfect recovery and sensitivity analysis of time encoded bandlimited signals," *IEEE Trans. Circuits Syst. I, Reg. Papers*, vol. 51, no. 10, pp. 2060–2073, Oct. 2004.

[35] N. S. Jayant and A. E. Rosenberg, "The preference of slope overload to granularity in the delta modulation of speech," *Bell Syst. Tech. J.*, vol. 50, no. 10, Dec. 1971.

[36] P. E. Allen and D. R. Holberg, *CMOS Analog Circuit Design*, 3rd ed. New York: Oxford Univ. Press, Aug. 2011.

[37] T. Jiang, W. Liu, F. Y. Zhong, C. Zhong, and P. Y. Chiang, "Single-channel, 1.25-GS/s, 6-bit, loop-unrolled asynchronous SAR-ADC in 40 nm-CMOS," in *IEEE Custom Integr. Circuits Conf.*, Sept. 2010, pp. 1–4.

[38] B. Razavi, *Design of Analog CMOS Integrated Circuits*, 1st ed. New York: McGraw-Hill, Aug. 2000.

[39] B. Wohlberg and P. Rodriguez, "An iteratively reweighted norm algorithm for minimization of total variation functionals," *IEEE Signal Process. Lett.*, vol. 14, no. 12, pp. 948–951, Dec. 2007.

Jun Zhou (S'10) received the B.S. degree in electrical engineering in 2007 from Fudan University, Shanghai, China. He received dual M.S. degrees in electrical engineering from Fudan University, Shanghai, China, and Royal Institute of Technology (KTH), Stockholm, Sweden, in 2010. He is currently working toward the Ph.D. degree at Texas A&M University, College Station, TX, USA.

He is a research assistant in Analog and Mixed Signal Center, Texas A&M University, College Station. His main research interests are in mixed signal processing and low-power VLSI design. He has presented one student best paper in IEEE International Symposium on Circuits and Systems (ISCAS).

Mario Ramirez is working toward the M.S. degree at the Analog and Mixed Signal Center at Texas A&M University, College Station.

His research interests comprise implementations of Compressed Sensing at circuit level and signal processing of biomedical signals.

Samuel Palermo (S'98–M'07) received the B.S. and M.S. degree in electrical engineering from Texas A&M University, College Station, in 1997 and 1999, respectively, and the Ph.D. degree in electrical engineering from Stanford University, Stanford, CA, in 2007.

From 1999 to 2000, he was with Texas Instruments Incorporated, Dallas, TX, where he worked on the design of mixed-signal integrated circuits for high-speed serial data communication. From 2006 to 2008, he was with Intel Corporation, Hillsboro, OR, where he worked on high-speed optical and electrical I/O architectures. In 2009, he joined the Electrical and Computer Engineering Department of Texas A&M University, College Station, where he is currently an assistant professor. His research interests include high-speed electrical and optical links, clock recovery systems, and techniques for device variability compensation.

Dr. Palermo is a member of Eta Kappa Nu. He has been on the IEEE CAS Board of Governors since 2011. He was a coauthor of the Jack Raper Award for Outstanding Technology-Directions Paper at the 2009 International Solid-State Circuits Conference.

Sebastian Hoyos (S'01–M'04) received the B.S. degree in electrical engineering from Pontificia Universidad Javeriana (PUJ), Bogota, Colombia, in 2000, and the M.S. and Ph.D. degrees in electrical engineering from the University of Delaware, Newark, in 2002 and 2004, respectively.

He was with Lucent Technologies Inc., Bogota, Colombia, from 1999 to 2000 for the Andean region in South America. Simultaneously, he was a lecturer with PUJ, where he lectured on microelectronics and control theory. During his M.S. and Ph.D. studies, he was with PMC-Sierra Inc., the Delaware Research Partnership Program, and the Army Research Laboratory Collaborative Technology Alliance in Communications and Networks. He was a Postdoctoral Researcher (2004–2006) with the Berkeley Wireless Research Center, Department of Electrical Engineering and Computer Sciences, University of California, Berkeley. He joined Texas A&M University, College Station, TX in 2006 where he is currently an Associate Professor with the Department of Electrical and Computer Engineering. His research interests include telecommunication systems, digital signal processing, and analog and mixed-signal processing and circuit design.